Rotational Analyses of Laser Induced Amplified Spontaneous Emission in the $E^2\Sigma^+(v = 1)$, $D^2\Sigma^+(v = 5)$, $L^2\Pi(v = 2)$, $B^2\Pi(v = 21)$, and $F^2\Delta(v = 0)$ States of NO

Koichi Tsukiyama

Department of Chemistry, Faculty of Science, Science University of Tokyo, Kagurazaka, Shinjuku, Tokyo 162, Japan

Received: April 30, 1996; In Final Form: July 23, 1996[⊗]

Amplified spontaneous emission (ASE) from single rotational levels of Rydberg states, $E^2\Sigma^+(v = 1)$, $D^2\Sigma^+(v = 5)$, and $F^2\Delta(v = 0)$, as well as valence states, $L^2\Pi(v = 2)$ and $B^2\Pi(v = 21)$, of NO molecules has been investigated. These states were populated through optical−optical double resonance excitation via the $A^2\Sigma^+$-($v' = 0$ and 1) states. ASE excitation spectra exhibited an excellent signal-to-noise ratio, demonstrating a high potential of the laser induced ASE (LIASE) technique as a novel spectroscopic technique for the study of excited states of small molecules. The rotational structure in dispersed ASE spectra have been fully resolved, which resulted in detailed information on the radiative ASE relaxation processes down to the $A^2\Sigma^+$ state.

I. Introduction

Amplified spontaneous emission (ASE) is highly directional radiation emitted in an extended medium with distributed population inversion of atoms and molecules in the absence of cavity mirrors.[1] The ASE process has been investigated in various laser media because it can interfere with laser oscillation. In the 1970s, the optically pumped dimer laser (OPL) was the subject of extensive experimental studies.[2] When the electronic transitions in homonuclear diatomic molecules such as Na_2 and I_2 are excited from the ground state to a level 2 in the excited state, a population inversion is formed between the level 2 and high-lying vibrational levels in the ground state, resulting in optically pumped stimulated emission (OPSE). The generation of ASE between electronically excited states has been also reported for Na_2.[3,4] Intense, directional ASE, with a defined threshold pumping intensity, has been observed at many infrared and visible wavelengths when Na_2 molecules are pumped with a single ultraviolet line.

Little attention has been paid to spectroscopic application of ASE in molecular systems until very recently. Westblom et al.[5] studied two-photon induced ASE (they used the term "stimulated emission" instead of ASE) from the $B^1\Sigma^+$ state of CO. They discussed the difference between ASE and fluorescence spectra corresponding to the $B^1\Sigma^+ \rightarrow A^1\Pi$ vibronic transitions. In our previous experiments,[6] we succeeded in observing ASE transitions of NO molecules which are based upon the inverted population between Rydberg states. Dispersed ASE spectra revealed the cascading radiative decay processes from the initially populated levels down to the $A^2\Sigma^+$ state. The results implied a high potential of the laser induced ASE (LIASE) as a novel spectroscopic tool for the highly excited states of small molecules.

In the present study, ASE relaxation processes from several lower Rydberg states, $E^2\Sigma^+(v = 1)$, $D^2\Sigma^+(v = 5)$, and $F^2\Delta(v = 0)$, as well as valence states, $L^2\Pi(v = 2)$ and $B^2\Pi(v = 21)$, have been investigated. Although fluorescence emission in these states except for the $E^2\Sigma^+$ and $F^2\Delta$ states has not been reported due to their predissociative character, strong ASE signals were observed. The rotational structure in dispersed ASE spectra was resolved completely, which provided us with detailed information on radiative relaxation processes among Rydberg and valence states.

II. Experimental Section

The experiments were performed in an optical−optical double resonance apparatus which is similar to that described in our previous publication.[6] A minor modification is that the UV radiations near 216 and 226 nm which induce the $A^2\Sigma^+(v' = 0$ and 1) $\leftarrow X^2\Pi_{3/2}(v'' = 0)$ vibronic transitions were obtained by second harmonic generation (SHG) instead of third harmonic generation (THG). The power density of the UV radiation was improved considerably, which brought us much higher spectral resolution.

A Q-switched YAG laser (Quanta Ray DCR-2A; pulse duration ∼5 ns operating at 10 Hz) pumped two dye lasers (Quanta Ray PDL-2) simultaneously. The output of the dye laser 1 (C-440 or C-460 in methanol) is frequency doubled by a BBO crystal ($5 \times 5 \times 6.5$ mm, Quantum Technology, cutting angle 50.2°). The resulting second harmonic is separated from the fundamental radiation by the use of a Pellin-Broca prism. The F_1 (e component; $J = N + 1/2$) levels of the $A^2\Sigma^+(v' = 0$ and 1) states are populated by selecting single rotational lines of the P_{12} branch of the $A^2\Sigma^+ \leftarrow X^2\Pi_{3/2}$ transition. The resonant condition was achieved by monitoring unresolved UV fluorescence corresponding to $A^2\Sigma^+(v' = 0$ or 1) $\rightarrow X^2\Pi(v'')$ by a solar blind photomultiplier tube (Hamamatsu R-166) placed at right angles to the laser beam.

The visible output of the second dye laser (5−500 μJ/pulse; bandwidth ∼0.3 cm^{-1}) interrogates higher excited states from the $A^2\Sigma^+(v' = 0$ or 1) state. The scanning ranges at around 600 nm for $E^2\Sigma^+(v = 1)$ and 560−565 nm for $F^2\Delta(v = 0)$, $L^2\Pi(v = 2)$, $B^2\Pi(v = 21)$, and $D^2\Sigma^+(v = 5)$ states are covered by Rh-640 and Rh-6G dyes, respectively. The visible laser beam is introduced into a quartz cell ($l = 10$ cm) filled with a few Torr of NO from the opposite direction to the UV beam. Near-infrared ASE generated in the same direction as the propagation of the UV laser, after being separated by a dichroic mirror and collimated properly, was detected with a photodiode (Hamamatsu B1720-02) with a current input amplifier (NF circuit design LI-76). A 25 cm monochromator (Nikon P-250; grating 600 grooves/mm blazed at 1000 nm) and later a 27.5 cm monochromator (Acton Research SP401) were employed to disperse the ASE.

[⊗] Abstract published in *Advance ACS Abstracts,* December 15, 1996.

S1089-5639(96)01218-2 CCC: $14.00

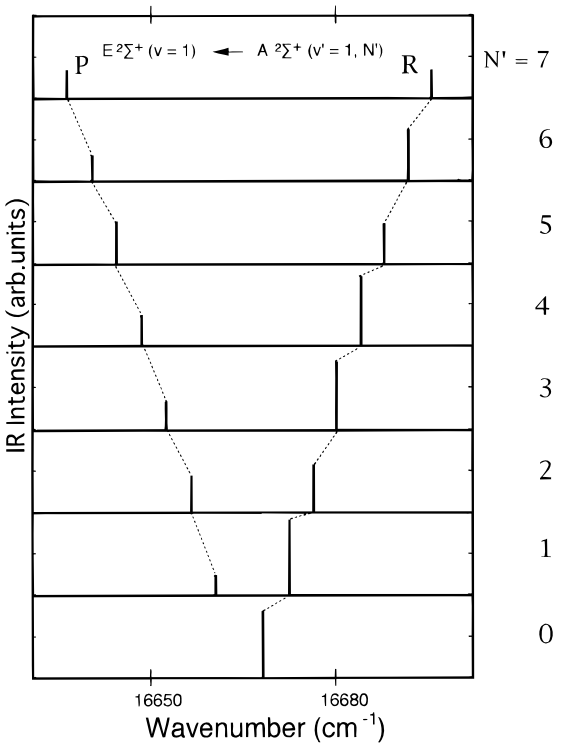

Figure 1. Rotational pattern in the ASE excitation spectrum for the $E^2\Sigma^+(v = 1) \leftarrow A^2\Sigma^+(v' = 1)$ transition.

Since the rotational structures of the excited states have already been analyzed in some detail, we did not attempt to calibrate the laser wavenumbers. The *J* numbering in the upper states is easily derived from the intervals between adjacent lines in the excitation spectra.

III. Results and Discussion

III-1. (4sσ)$E^2\Sigma^+(v = 1)$ State. The rotational structure of the $E^2\Sigma^+$ state has been thoroughly analyzed through Fourier transform spectrometry[7] of the $E^2\Sigma^+ \rightarrow D^2\Sigma^+$ and $E^2\Sigma^+ \rightarrow A^2\Sigma^+$ bands and double resonance laser spectroscopy[8,9] via the $A^2\Sigma^+$ state. Because the pump (UV) laser has selected a single rotational level, the excitation spectrum for the $E^2\Sigma^+ \leftarrow A^2\Sigma^+$ transition consists of one or two lines corresponding to the R and P branches allowed for a $^2\Sigma^+ - ^2\Sigma^+$ transition. Figure 1 depicts such a Fortrat type spectral pattern for the $E^2\Sigma^+(v = 1) \leftarrow A^2\Sigma^+(v' = 1)$ band. The wavenumbers were calculated from published term values for these states.[7]

Figure 2 illustrates the dispersed ASE spectrum obtained when the $E^2\Sigma^+(v = 1, N = 6, F_1)$ level is populated through the excitation of the $R_{11}(5)$ line. The trace includes two electronic bands, namely, $E \rightarrow D(1,1)$ around 1300 nm, and $D \rightarrow A(1,1)$ around 1100 nm. The former band is composed of a pair of rotational lines which are assignable to R(5) and P(7). The rotational quantum numbers in parentheses represent those of the lower state, i.e., $D^2\Sigma^+(v = 1)$. The latter band consists of four lines which are attributable to the cascading radiative relaxation down to the $A^2\Sigma^+(v = 1)$ state as shown in Figure 3. The observation of these four ASE transitions is justified because the population inversion between $D^2\Sigma^+$ and $A^2\Sigma^+$ states is maintained except for $N = 5$ under collisionless conditions. Because the oscillator strength of the $E \rightarrow C$ band is 2 orders of magnitude smaller than that of the $E \rightarrow D$ band,[10] the former band near 1175 nm is absent in Figure 2.

The intensity of the spontaneous fluorescence in the P and R branches of $D \rightarrow A$ following $E \rightarrow D$ can be evaluated by multiplying the appropriate Hönl−London factors of the two

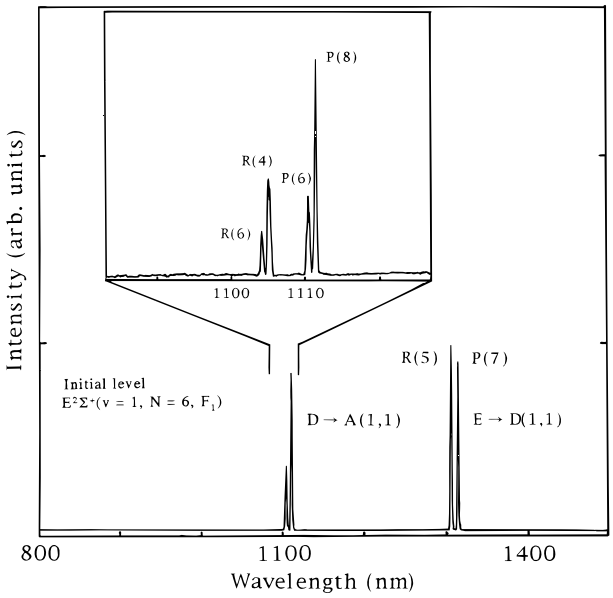

Figure 2. Dispersed ASE spectrum from the $E^2\Sigma^+(v = 1, N = 6, F_1)$ level.

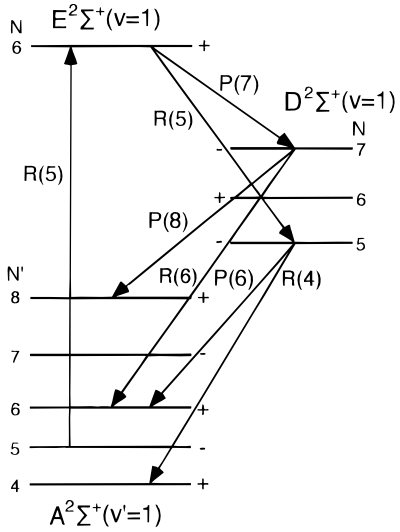

Figure 3. Cascading ASE relaxation process from the $E^2\Sigma^+(v = 1, N = 6, F_1)$ level.

consecutive transitions. Comparing the calculated ratio, R(6):R(4):P(6):P(8) = 49:30:36:56, with the experimental one (see the inset of Figure 2), one notices that the calculation overestimates the intensity of the R(6) line. The disagreement might be due to the suppression of the R(6) ASE transition by the P(6) transition which has a common lower level.

III-2. $L^2\Pi(v = 2)$ Valence State. The $L^2\Pi$ valence state has been the subject of both experimental[11−14] and theoretical[15] investigations. Because all the vibrational levels of the $L^2\Pi$ state are predissociative, no fluorescence emission has been reported so far. Hereafter we adopt the vibrational numbering of the $L^2\Pi$ state assigned by Gallusser and Dressler.[15] In the ASE excitation spectrum for the $L^2\Pi_{3/2}(v = 2) \leftarrow A^2\Sigma^+(v' = 1)$ band, a strong Q branch and a rather weak R branch are identified as shown in Figure 4. No corresponding P branch was discovered, which contradicts the usual selection rules for the $^2\Pi - ^2\Sigma^+$ system. This brings out a striking contrast to the REMPI spectrum for the $L^2\Pi(v = 8) \leftarrow A^2\Sigma^+(v' = 1)$ transition in which P, Q, and R branches appear with similar intensities.[12] Several lines near 17 770 cm^{-1} originate from the $K^2\Pi(v = 0)$ Rydberg state.

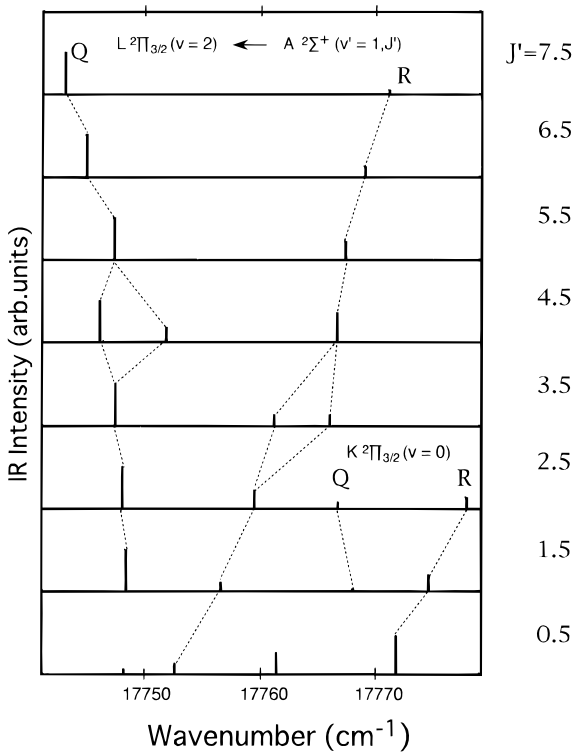

Figure 4. Rotational pattern in the ASE excitation spectrum for the $L^2\Pi_{3/2}(v = 2) \leftarrow A^2\Sigma^+(v' = 1)$ transition.

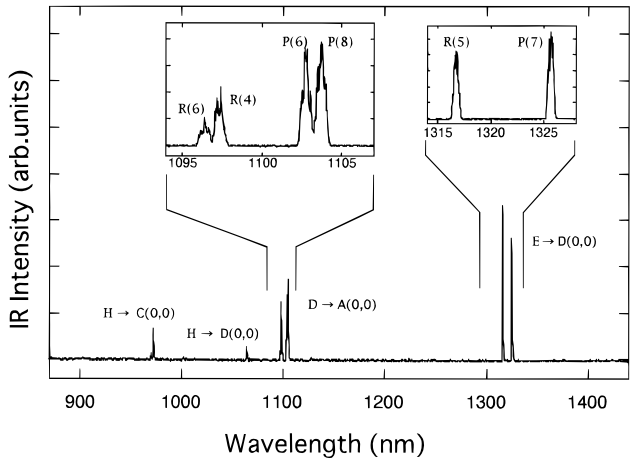

Figure 5. Dispersed ASE spectrum from the $L^2\Pi_{3/2}(v = 2, J = 6.5)$ level.

Several cascading ASE processes from the $L^2\Pi_{3/2}(v = 2, J = 6.5, -)$ state are identified in Figure 5.

1. The bands at around 1320 and 1100 nm are analyzed to be E → D(0,0) and D → A(0,0) transitions, respectively. The rotational structure is the same as that described in Figure 2 for the 1−1 transition, except that the E → D and D → A bands are slightly shifted to shorter and longer wavelengths, respectively, owing to the slightly anomalous vibrational frequency of the D state. Because there are no populations in the $D^2\Sigma^+$ and $A^2\Sigma^+$ ($v = 0$) states, all the allowed rovibronic transitions appear in the dispersed ASE spectrum.

2. The band in the vicinity of 1060 nm is known to belong to the $H^2\Sigma^+$, $H'\,^2\Pi \rightarrow D^2\Sigma^+$ transition.[16] Recently, the HH′ → D(0,0) band has been investigated in great detail by Fourier transform emission spectrometry.[17] With the aid of this high-resolution spectrum, we found that the $H^2\Sigma^+(v = 0, J = 6.5, +) \rightarrow D^2\Sigma^+(v = 0, J = 5.5, -)$ transition is in perfect agreement with the single line at 1062.8 nm (9409.3 cm^{-1}) in Figure 5.

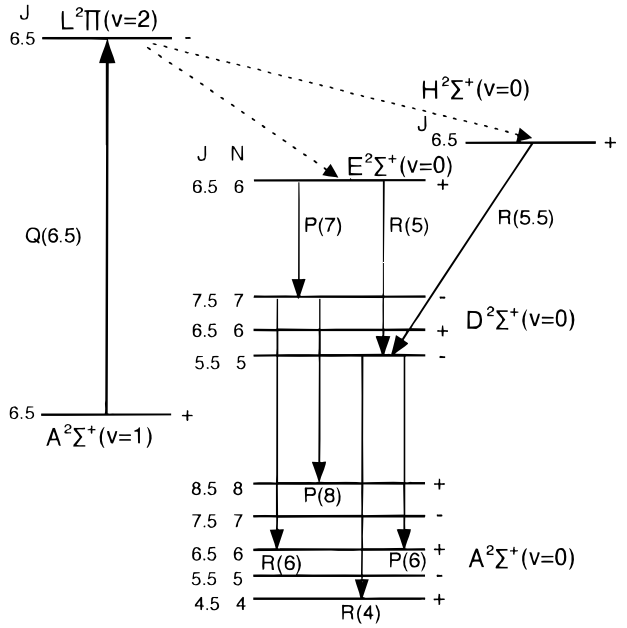

Figure 6. Cascading ASE relaxation process from the $L^2\Pi_{3/2}(v = 2, J = 6.5)$ level.

TABLE 1: Mixing Coefficients of T_x, T_y, and T_z States and Fractional Weights of C1 and C2[a]

state	J	C1	C2	C3	Γ_{C1}	Γ_{C2}
T_x	1.5	0.99	−0.05	−0.16	0.98	
	2.5	0.98	−0.06	−0.18	0.96	
	3.5	0.96	−0.05	−0.25	0.92	
	4.5	0.84	−0.08	−0.53	0.71	
	5.5	0.43	−0.11	−0.90	0.18	
	6.5	0.19	−0.08	−0.97	0.04	
T_y	1.5	0.05	−0.99	+0.08	∼0	0.98
	2.5	0.18	−0.85	+0.48	0.03	0.72
	3.5	0.35	−0.42	+0.83	0.12	0.18
	4.5	0.62	−0.20	+0.75	0.38	0.04
	5.5	0.90	−0.07	+0.42	0.81	∼0
	6.5	0.96	−0.02	+0.21	0.92	∼0
T_z	1.5	0.23	+0.23	+0.95	0.05	0.05
	2.5	0.19	+0.47	+0.86	0.04	0.22
	3.5	0.10	+0.84	+0.52	0.01	0.71
	4.5	0.04	+0.96	+0.29	∼0	0.92
	5.5	0.02	+0.98	+0.19	∼0	0.96
	6.5	0.01	+0.99	+0.12	∼0	0.98

[a] Taken from ref 19.

No transitions from $H'\,^2\Pi^{\pm}(v = 0)$ to $D^2\Sigma^+(v = 0)$ are seen in the spectrum. Figure 6 summarizes the cascading pathways from the $L^2\Pi(v = 2, J = 6.5, -)$ state.

The above assignment is supported by the following two observations. First, if the ASE from the $H^2\Sigma^+(v = 0)$ state populates rotational levels other than $J = 7.5$ and 5.5 in the $D^2\Sigma^+(v = 0)$ state, more than four rotational lines would be expected in the D → A ASE spectrum. No signs of extra lines were found in the set of Figure 5. Second, the single line at 970.1 nm (10 308.2 ± 2.0 cm^{-1}) is in good agreement with the wavenumbers of the allowed transitions[18] from $H^2\Sigma^+(v = 0, J = 6.5, +)$ to $C^2\Pi(v = 0, T_z, J = 5.5, -)$ at 10 307.1 cm^{-1} and to $C^2\Pi(v = 0, T_y, J = 6.5, -)$ at 10 306.5 cm^{-1}. It has long been established that the $C^2\Pi(v = 0)$ state is mixed with $B^2\Pi(v = 7)$; the homogeneous interaction of the two states yields these strongly perturbed spin components usually labeled T_x, T_y, and T_z.[19] Table 1 lists the mixing coefficients of $C^2\Pi_{1/2}$(C1), $C^2\Pi_{3/2}$(C2), and $B^2\Pi_{3/2}$(B2) wave functions in the noncrossing components T_x, T_y, and T_z. Γ_{C1} and Γ_{C2} represent the fractional weights of C1 and C2 states, respectively. Transitions to the T_x component are unlikely to occur because

the higher rotational levels ($J \geq 5.5$) are mostly $B^2\Pi$ with only minor contributions from $C^2\Pi$. A clearer example concerning the effect of perturbation in the $C^2\Pi(v = 0)$ state on the rotational structure will be presented in section III-4.

When the $H^2\Sigma^+(v = 0)$ state is directly populated by the laser excitation, $D^2\Sigma^+(v = 0)$ and $C^2\Pi(v = 0)$ states are the first destinations in the cascading ASE decay processes.[6] Because the $(4d\sigma)H^2\Sigma^+ \rightarrow (4s\sigma)E^2\Sigma^+$ transition is forbidden in the united atom limit, the H → E ASE channel is not open. Hence, as drawn by the dotted arrow in Figure 6, the $E^2\Sigma^+(v = 0)$ state must be populated not via $H^2\Sigma^+(v = 0)$ but directly from the $L^2\Pi(v = 2)$ state. On the other hand, the first steps of the cascading ASE relaxation from the $(4p\pi)K^2\Pi$ state begin with transitions to the $E^2\Sigma^+$ and $H^2\Sigma^+$, $H'\,^2\Pi$ states with $\Delta v = 0$.[6] The observation of L → E(2,0) as well as L → H(2,0) ASE decays is a clear demonstration that the Rydberg $K^2\Pi(v = 0)$ state dominates the ASE process in the valence $L^2\Pi(v = 2)$ state. Gallusser and Dressler[15] pointed out that the effective interaction between $L^2\Pi(v = 2)$ and $K^2\Pi(v = 0)$ is dominated by a third order contribution, namely, a perturbation path $L2 + Cv + Bv + K0$; the matrix element which couples the two vibronic levels directly has a magnitude of as low as $H(L2 \sim K0) = 0.07$ cm^{-1}. In spite of the relatively large first order interaction energy of $H(L2 \sim C5) = 40$ cm^{-1}, no ASE transitions based on the interaction with the $C^2\Pi(v = 5)$ Rydberg state, such as $L^2\Pi(v = 2) \rightarrow A^2\Sigma^+(v = 5)$, were seen in Figure 6.

It is interesting to point out that C → A ASE near 1240 nm could be detected in the excitation of lower J levels of the $L^2\Pi$ state; the ratio of the C → A intensity to the H → C intensity decreases from ~0.5 at $J = 2.5$ to ~0 at $J = 6.5$. This is in accordance with the predissociation of the $C^2\Pi(v = 0)$ state. The T_y ($J = 3.5$) and T_z ($J = 2.5$) levels are located above the first dissociation limit.[20] Since the nonradiative channel destroys the population inversion between $C^2\Pi$ and $A^2\Sigma^+$ states, the population inversion density cannot sufficiently grow to reach the ASE threshold.

It is worth commenting on the enhancement of the Q branch in the ASE excitation spectrum of the $L^2\Pi_{3/2}(v = 2) \leftarrow A^2\Sigma^+(v' = 1)$ transition. This anomalous intensity pattern may be due to the interaction with the $3d\sigma$, π $H^2\Sigma^+$, $H'\,^2\Pi(v = 1)$ state located ~750 cm^{-1} above the $L^2\Pi_{3/2}(v = 2)$ state. The unusual rotational structure, that is, R for $H^2\Sigma^+ \leftrightarrow {}^2\Sigma^+$, P for $H'\,^2\Pi^+ \leftrightarrow {}^2\Sigma^+$, and Q for $H'\,^2\Pi^- \leftrightarrow {}^2\Sigma^+$ of the emission[21] and excitation[22] bands with the 3d complex as the upper state directly reveals the partial case (d) structure of this complex. We believe that the $H'\,^2\Pi^-$ character (f1 component; positive for odd $J - 1/2$) in the $L^2\Pi_{3/2}(v = 2)$ state is the origin of the enhancement of the Q branch.

III-3. $(3p\sigma)D^2\Sigma^+(v = 5)$ and Valence $B^2\Pi(v = 21)$ States. The absorption spectrum of the $D^2\Sigma^+(v = 5) \sim B^2\Pi(v = 21)$ mixed states from the ground state was analyzed by Lagerqvist and Miescher.[11,23] Using their term values, the rotational assignments for the LIASE excitation spectrum have been made as shown in Figure 7. The homogeneous perturbation between the $H^2\Sigma^+(v = 1)$ and $D^2\Sigma^+(v = 5)$ states is presumably responsible for the absence of a P branch in the $D^2\Sigma^+(v = 5) \leftarrow A^2\Sigma^+(v' = 1)$ transition; in the $H^2\Sigma^+ \leftrightarrow {}^2\Sigma^+$ band, the R branch is much stronger than P branch. This interaction explains consistently why the inter-Rydberg transition with $\Delta v = 4$ appears with appreciable intensity.

The splitting between e and f components of the $D^2\Sigma^+(v = 5)$ state is observed for $N \geq 4$. The ASE pathway in the $D^2\Sigma^+(v = 5, N = 5)$ level is illustrated in Figure 8a. The lower electronic state was assigned as the $A^2\Sigma^+(v = 5)$ state. Although the $D^2\Sigma^+(v = 1)$ and $A^2\Sigma^+(v = 5)$ states overlap,

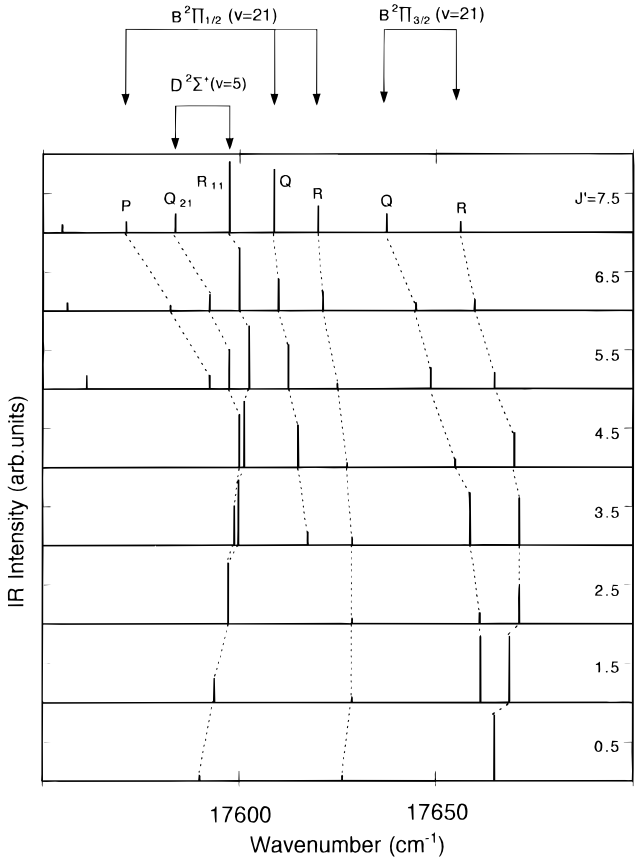

Figure 7. Rotational pattern of the ASE excitation spectrum in the $D^2\Sigma^+(v = 5) \sim B^2\Pi(v = 21) \leftarrow A^2\Sigma^+(v' = 1)$ transition. Rotational assignments are based on transition energies from the ground state tabulated in Tables I and II in ref 11.

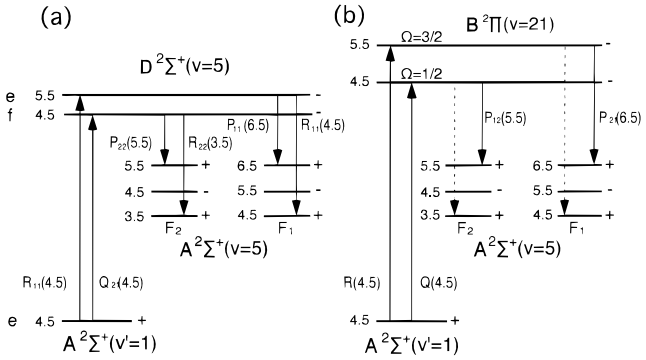

Figure 8. Cascading ASE relaxation process from the $D^2\Sigma^+(v = 5)$ and $B^2\Pi(v = 21)$ states.

our rotational analyses find no signs of transitions to the $D^2\Sigma^+(v = 1)$ state, which complies with the absence of the cascading D → A(1,1) ASE in the dispersed ASE spectrum. The rotational structure from the e component (F_1) exhibits both $R_{11}(4.5)$ and $P_{11}(6.5)$ lines with the former being about twice as intense as the latter. The ASE transitions from the f component (F_2) also consists of two lines, namely, $R_{22}(3.5)$ and $P_{22}(5.5)$, though the former is more than 1 order of magnitude stronger than the latter. Alternative assignments of $P_{11}(6.5)$ and $R_{22}(3.5)$ as $Q_{12}(5.5)$ and $Q_{21}(4.5)$, respectively, seem unlikely on the basis of the observed intensities, considering that the ASE process is dominated by the $\Sigma^+ - \Sigma^+$, $\Delta v = 0$, inter-Rydberg transition. As suggested earlier, the mixing with the $H^2\Sigma^+(v = 1)$ state may cause the enhancement of R branch transitions.

The ASE excitation spectrum for the $B^2\Pi(v = 21)$ state (Figure 7) exhibits P, Q, and R branches. The P branch is very

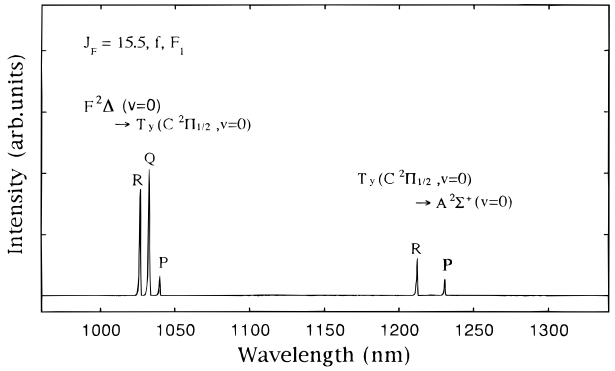

Figure 9. Dispersed ASE spectrum from the $F^2\Delta(v = 0, J = 15.5, f, F_1)$ level.

weak and not detected for $\Omega = 3/2$. The ASE transition, as depicted in Figure 8b, can be attributed to the P branch. Corresponding R branches, illustrated as dotted arrows, are much weaker than P branches; for instance, the intensity of the $R_{21}(4.5)$ line is about 1/50 of $P_{21}(6.5)$. Neither do we see R line emission from $J = 4.5$ or 3.5 of the $B^2\Pi_{3/2}(v = 21)$ state. This anomalous intensity distribution is not well understood at the present stage.

III-4. (3dδ)$F^2\Delta(v = 0)$ State. The electronic structure of the (3dδ)$F^2\Delta$ state and the interaction with the nearby valence $B'\,^2\Delta$ state was thoroughly investigated by Jungen.[24] The fluorescence lifetime of the $F^2\Delta(v = 0)$ state was measured to be 31.2 ns, implying that predissociation is negligible.[25] In spite of the forbidden character of the $F^2\Delta \leftarrow A^2\Sigma^+$ transition ($\Delta\Lambda = 2$), this band was employed to probe the rotational distribution of the nascent NO in the $A^2\Sigma^+$ state produced in photodissociation of the rare gas−NO van der Waals complexes.[26] In the present study, the $F^2\Delta(v = 0) \leftarrow A^2\Sigma^+(v = 0)$ band was observed with appreciable intensity.

Several features of the excitation spectra are addressed below.

1. The excitation spectrum consists of an intense Q_{11} branch, and weaker P_{11} and R_{11} branches of equal intensities. This pattern is identical with that measured with ion-current detection.[26]

2. Transitions to higher rotational levels ($J_F \geq 10.5$) are much stronger (2 orders of magnitude at most) than those to lower rotational levels ($J_F \leq 5.5$).

3. At higher probe laser power, the weak R_{21} branch is detectable. Q_{21} and P_{21} branches overlap with R_{11} and Q_{11} branches, respectively, because the $F^2\Delta$ and $A^2\Sigma^+$ states belong to Hund's case b. This could mean that the F_1 and F_2 components are populated simultaneously. For the measurement of dispersed ASE spectra, laser power was reduced to achieve the selective excitation to the F_1 component via the Q_{11} branch.

The ASE relaxation process begins with the $F^2\Delta(v = 0) \rightarrow C^2\Pi(v = 0)$ band which is the only dipole-allowed inter-Rydberg transition. As mentioned in section III-2, the homogeneous interaction between $C^2\Pi$ and $B^2\Pi$ yields three non-crossing spin components labeled T_x, T_y, and T_z. Because the perturbation is strongest for low rotation ($J_C \leq 5.5$), it seems reasonable to deal separately with the low-J and high-J ($J_C \geq 6.5$) regions.

III-4-1. High-J Region. In the high-J region, T_x, T_y, and T_z convert to $B^2\Pi_{3/2}$ (denoted B2 by Ackermann and Miescher[19]), $C^2\Pi_{1/2}$ (C1) and $C^2\Pi_{3/2}$ (C2), respectively. A typical dispersed ASE spectrum is depicted in Figure 9; similar spectral patterns were observed at all J_F from 12.5 to 18.5. A series of peaks around 1030 and 1220 nm are attributed to $F^2\Delta(v = 0) \rightarrow C^2\Pi(v = 0)$ and $C^2\Pi(v = 0) \rightarrow A^2\Sigma^+(v = 0)$, respectively. The rotational analysis as shown in Figure 10 was accomplished

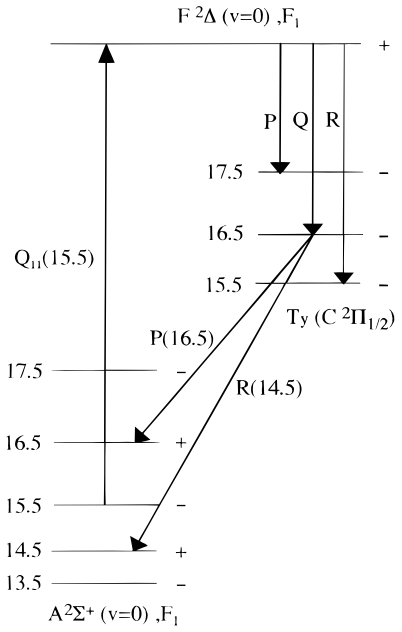

Figure 10. Cascading ASE relaxation process from the $F^2\Delta(v = 0, J = 15.5, f, F_1)$ level.

rather easily because accurate term values for $C^2\Pi(v = 0)$[27] and $F^2\Delta(v = 0)$[28] states have been established; three lines correspond to P_{1y}(weak), Q_{1y}, and R_{1y} (strong) branches from $F^2\Delta$ to C1(T_y) while a pair of lines corresponds to P_{y1} and R_{y1} branches of the cascading ASE transition from C1 to $A^2\Sigma^+$. The transitions to T_z cannot reproduce the peak positions. T_z goes to C2 in the high-J limit; accordingly the $F_1 \rightarrow T_z$ transition corresponds to $F_1 \rightarrow F_2$. Such spin−flip transitions are forbidden under Hund's case b.

The intensity ratio of C → A to F → C is ∼0.3 at $J_F = 15.5$ (Figure 9), ∼0.1 at 14.5 and <0.02 at 12.5. Below 11.5, no C → A transitions are detectable. This is in sharp contrast with the observation described in section III-2. One possible explanation is that the population inversion density between the $C^2\Pi(v = 0)$ and $A^2\Sigma^+(v = 0)$ states arising from ASE in the $F^2\Delta(v = 0)$ state is not high enough to induce the following cascading ASE. Due to the forbidden character of the $F^2\Delta \leftarrow A^2\Sigma^+$ transition, particularly at low J, the absolute number density in the $F^2\Delta$ state may be much lower than for the other transitions described so far.

III-4-2. Low-J Region. Figure 11 summarizes the ASE peak locations and approximate intensities originating in the $F^2\Delta(v = 0, 2.5 \leq J_F \leq 6.5, F_1)$ levels. For $J_C \leq 4.5$, T_x is almost purely C1 whereas for $J_C \geq 5.5$, T_y possesses the largest fractional weight of C1 wave function (see Table 1). This switching is in perfect agreement with the ASE rotational pattern in Figure 11; the spectrum is produced from two lines attributed to R_{1x} and Q_{1x} for $J_C \leq 4.5$ while R_{1y} and Q_{1y} lines are dominant for $J_C \geq 5.5$. Note that $R_{1x}(5.5)$ and $Q_{1x}(5.5)$ lines are absent.

III-4-3. ASE from F_2 levels. We found that the Q_{2z} branch is dominant in ASE transitions from the F_2 components of the $F^2\Delta(v = 0, 4.5 \leq J_F \leq 8.5)$ state. These levels are populated through the R_{21} branch transition of the $F^2\Delta \leftarrow A^2\Sigma^+$ band following $A^2\Sigma^+$ state excitation via the $Q_{22} + R_{12}$ branch of the $A^2\Sigma^+ \leftarrow X^2\Pi$ band. This observation is consistent with the almost exclusive C2 fractional weight in T_z for $J \geq 4.5$. It should be emphasized that the above branch pattern is totally different from the fine structure in the spectrum of the electronic NO laser.[29,30] Miescher[30] reported two strong laser lines, namely, $R_{2y}(5.5)$ and $Q_{2y}(5.5)$. The presence of these two lines was interpreted as evidence for the predissociative character of

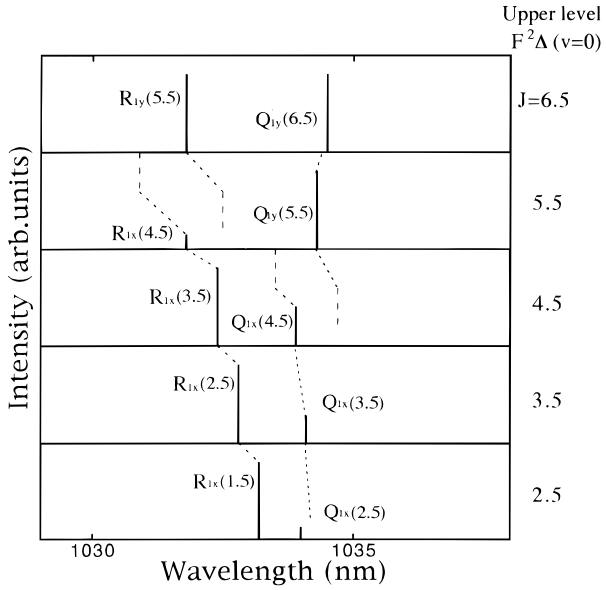

Figure 11. Rotational pattern in the dispersed ASE spectrum corresponding to the $F^2\Delta(v = 0) \rightarrow C^2\Pi(v = 0)$ transition at low J region.

the lower level. The mechanism of lasing in a cavity must be different from that of ASE without a cavity.

IV. Conclusion

We applied the LIASE technique to the Rydberg states, $E^2\Sigma^+(v = 1)$, $D^2\Sigma^+(v = 5)$, and $F^2\Delta(v = 0)$, as well as the valence states, $L^2\Pi(v = 2)$ and $B^2\Pi(v = 21)$ states of NO molecules. Significant findings in the present study are as follows:

1. For the excitation of $E^2\Sigma^+(v = 1)$, the cascading ASE process is E → D(1,1) followed by D → A(1,1). The rotational structures of the excitation and of the emission bands are in agreement with the usual selection rules for $\Sigma^+-\Sigma^+$ transitions because the $E^2\Sigma^+(v = 1)$ state is isolated.

2. The first steps of the ASE relaxation processes from $L^2\Pi(v = 2)$ are L → E(2,0) and L → H(2,0). No signs of the transition to the $H'\,^2\Pi(v = 0)$ state were found. The driving force of these transitions is the perturbation of $L(v = 2)$ by the nearby $K^2\Pi(v = 0)$ state. Mixing of the $H'\,^2\Pi(v = 1)$ state with $L^2\Pi(v = 2)$ is suggested as the cause of the anomalous intensity pattern in the excitation spectrum.

3. The ASE pathways from the $D^2\Sigma^+(v = 5) \sim B^2\Pi(v = 21)$ mixed states are direct transitions down to the $A^2\Sigma^+(v = 5)$ state. The interaction of the $H^2\Sigma^+$ state with the $D^2\Sigma^+$ state is proposed for the enhancement of the R branch in both excitation and emission spectra.

4. The excitation to the $F^2\Delta(v = 0)$ state produces ASE down to the $C^2\Pi(v = 0)$ state. The mixing of this state with $B^2\Pi_{3/2}(v = 7)$ explains successfully the rotational pattern in the ASE spectrum which is entirely different from that of the known NO lasing transitions.[29,30]

The present study, together with our previous investigation on the higher Rydberg members of NO, demonstrates the tremendous potential of LIASE as a novel laser spectroscopic technique. In particular, its applicability to weakly predissociative states would appear to be one of the main advantages. However, further experiments are required for the quantitative treatment of the signal intensity. For example, the intensity of relatively weak peaks in the ASE excitation spectrum, such as the $B^2\Pi_{1/2}(v = 21) \leftarrow A^2\Sigma^+(v' = 1)$ transition, is difficult to reproduce. Furthermore, as pointed out in section III-1, the intensity pattern of ASE differs from that of spontaneous fluorescence. Similar spectral difference between LIASE and laser induced fluorescence was reported in vibronic bands of CO.[5,31] The understanding of those phonomena, presumably in part related to the ASE threshold conditions, will be one of the future subjects.

Finally, a brief perspective on the sensitivity of the ASE technique is given here. For this purpose, the $E^2\Sigma^+(v = 0) \leftarrow A^2\Sigma^+(v' = 0)$ excitation spectrum was taken under pulsed-jet conditions. Employing equations given by Rettner et al.,[32] several relevant parameters are evaluated: NO density in the jet $<1 \times 10^{15}/cm^3$; rotational temperature ~ 20 K; effective path length $L \sim 5$ mm; laser power $P_{UV} < 100$ μJ, $P_{vis} < 1$ μJ/pulse. Under these conditions, a signal-to-noise ratio greater than 2000 was easily achieved, which seems to promise the future use of this novel spectroscopic method not only in studies of highly excited states of molecules but also in nondestructive analyses of complex chemical systems.

Acknowledgment. This work is partly supported by the Morino Foundation, a Grant-in-Aid (No. 07640697) and that on Priority-Area-Research "Photoreaction Dynamics" (No. 07228268) from the Ministry of Education, Science, Sports and Culture, Japan. The author thanks Prof. K. P. Huber for communicating term values of the $F^2\Delta(v=0)$ state and for critical reading of the manuscript. I am greatly indebted to A. Sugita and S. Dobashi for their help in the experiment.

References and Notes

(1) Siegman, A. E. *Lasers*; Oxford University Press: Oxford, 1986.
(2) Wang, Z. G.; Xia, H. R. *Molecular and Laser Spectroscopy*; Springer Series in Chemical Physics 50; Springer: Berlin, 1986.
(3) Wang, Z. G.; Xia, H. R.; Ma, L. S.; Lin, Y. Q.; Cheng, I. S. *Appl. Phys.* **1985**, *B37*, 233.
(4) Wang, Z. G.; Wang, Y. C.; Morgan, G. P.; Schawlow, A. L. *Opt. Commun.* **1984**, *48*, 398.
(5) Westblom, U.; Agrup, S.; Aldén, M.; Hertz, H. M.; Goldsmith, J. E. M. *Appl. Phys.* **1990**, *B50*, 487.
(6) Ishii, J.; Uehara, K.; Tsukiyama, K. *J. Chem. Phys.* **1996**, *108*, 499.
(7) Amiot, C.; Verges, J. *Phys. Scr.* **1982**, *20*, 422.
(8) Meijer, G.; Ebben, M.; Ter Meulen, J. *J. Chem. Phys.* **1988**, *127*, 173.
(9) Ashfold, M. N. R.; Dixon, R. N.; Prince, J. D.; Tutcher, B.; Western, C. M. *J. Chem. Phys.* **1986**, *82*, 1257.
(10) Gallusser, R.; Dressler, K. *J. Appl. Math. Phys.* (*ZAMP*) **1971**, *22*, 792.
(11) Lagerqvist, A.; Miescher, E. *Can. J. Phys.* **1966**, *44*, 1525.
(12) Cheung, W. Y.; Chupka, W. A.; Colson, S. D.; Gauyacq, D.; Avouris, P.; Wynne, J. J. *J. Phys. Chem.* **1986**, *90*, 1086.
(13) Ebata, T.; Mikami, N.; Ito, M. *J. Chem. Phys.* **1983**, *78*, 1132.
(14) Dressler, K.; Miescher, E. *J. Chem. Phys.* **1981**, *75*, 4310.
(15) Gallusser, R.; Dressler, K. *J. Chem. Phys.* **1982**, *76*, 4311.
(16) Miescher, E.; Huber, K. P. *Spectroscopy*; Ramsay, D. A., Ed.; Physical Chemistry Series Two 3; Butterworths: London, 1976.
(17) Bernard, A.; Effantin, C.; d'Incan, J.; Amiot, C.; Verges, J. *Mol. Phys.* **1991**, *73*, 221.
(18) Rottke, H.; Zacharias, H. *J. Chem. Phys.* **1985**, *83*, 4831.
(19) Ackermann, F.; Miescher, E. *J. Mol. Spectrosc.* **1969**, *31*, 400.
(20) Tsukiyama, K.; Munakata, T.; Tsukakoshi, M.; Kasuya, T. *Chem. Phys.* **1988**, *121*, 55.
(21) Miescher, E. *Can. J. Phys.* **1971**, *49*, 2350.
(22) Ishii, J.; Uehara, K.; Tsukiyama, K. *J. Chem. Phys.* **1995**, *102*, 9174.
(23) Jungen, C.; Miescher, E. *Can. J. Phys.* **1968**, *46*, 987.
(24) Jungen, C. *Can. J. Phys.* **1966**, *44*, 3197.
(25) Hart, D. J.; Hepburn, J. W. *J. Chem. Phys.* **1987**, *86*, 1733.
(26) Sato, K.; Achiba, Y.; Nakamura, H.; Kimura, K. *J. Chem. Phys.* **1986**, *85*, 1418.
(27) Amiot, C.; Verges, J. *Phys. Scr.* **1982**, *25*, 302.
(28) Huber, K. P. Private communication.
(29) Jungen, C.; Miescher, E.; Suter, R. *Phys. Lett.* **1966**, *21*, 36.
(30) Miescher, E. *J. Mol. Spectrosc.* **1974**, *53*, 302.
(31) Tsukiyama, K. *Appl. Phys. B* **1996**, *63*, 311.
(32) Rettner, C. T.; Marinero, E. E.; Zare, R. N.; Kung, A. H. *J. Phys. Chem.* **1984**, *88*, 4459.